North Indian Ocean tropical cyclone activity in CMIP5 experiments: Future projections using a model-independent detection and tracking scheme

Samuel S. Bell[1],

Savin S. Chand[1],

Kevin J. Tory[2],

Hua Ye[2]

Chris Turville[1]

[1] Centre for Informatics and Applied Optimization, Federation University Australia, Ballarat 3357, Australia
[1] Research and Development Branch, Bureau of Meteorology, Melbourne 3001, Australia

Corresponding Author e-mail: ss.bell@federation.edu.au

Keywords: Tropical cyclone, track, north indian ocean, model projection, climate change, Asian monsoon, Bay of Bengal, Arabian Sea

This article has been accepted for publication and undergone full peer review but has not been through the copyediting, typesetting, pagination and proofreading process which may lead to differences between this version and the Version of Record. Please cite this article as doi: 10.1002/joc.6594

Abstract

The sensitivity of tropical cyclone (TC) projection results to different models and the detection and tracking scheme used is well established. In this study, future climate projections of TC activity in the North Indian Ocean (NIO) are assessed with a model- and basin-independent detection and tracking scheme. The scheme is applied to selected models from the Coupled Model Intercomparison Project Phase 5 (CMIP5) experiments forced under the historical and Representative Concentration Pathway 8.5 (RCP8.5) conditions. Most models underestimated the frequency of early season (April-June) TCs and contained genesis biases equatorward of ~7.5°N in comparison to the historical records. TC tracks detected in reanalysis and model data were input to a clustering algorithm simultaneously, with two clusters in the Arabian Sea and two in the Bay of Bengal (k=4). Projection results indicated a slight decrease of overall TC genesis frequency in the NIO, with an increase of TC genesis frequency in the Arabian Sea (30–64%) and a decrease in the Bay of Bengal (22–43%), consistent between clusters in each of these sub-regions. These changes were largely due to changes in the pre-monsoon season (April-June) where Bay of Bengal TCs significantly decreased, consistent with changes in vertical ascent. Northern Arabian Sea TCs significantly increased during the pre-monsoon season, consistent with changes in vertical wind shear and relative humidity. There was a projected increase of TC frequency in the post-monsoon season (October-December), consistent with changes in relative humidity and vertical ascent, although not all clusters followed this trend; noting a different response in the southern Bay of Bengal. In turn, these projections caused changes to the climate averaged TC track density, including a decrease (up to 2 TCs per decade) affecting the eastern coast of India and a small increase (up to 0.5 TCs per decade) affecting eastern Africa, Oman and Yemen.

1. Introduction

Tropical cyclone (TC) genesis location and track direction are important characteristics when considering TC landfall densities. This elevates the need to determine how these TC characteristics are impacted by changes in the climate. In terms of dedicated studies, the North Indian Ocean (NIO) TC basin has received scant attention compared to other basins in the literature. Although the NIO basin is the least active compared to the other basins, and therefore intense TCs are rarely observed, it is extremely vulnerable to TC impacts due to its densely populated coastal regions, as indicated by TC Bhola in 1970, the deadliest TC in history (Emanuel 2005).

The NIO basin experiences two active periods of TC activity, pre-monsoon (April to June) and post-monsoon (October to December) with a lull in activity during the peak monsoon season (July to September). Two sub-regions can be defined divided by the Indian sub-continent that experience asymmetric activity (Sattar and Cheung 2019), the more active Bay of Bengal to the east (Alam et al. 2003) where TCs can impact the coastlines of India and Bangledesh (Singh et al. 2000), and the quieter Arabian Sea to the west (Mohapatra et al. 2014) where TCs can sometimes reach the Arabian Peninsula (i.e., Oman and Yemen, see Fig. 1 for geographical location of these countries).

A significant climate projection study on TC frequency in the NIO is that of Murakami et al. (2013), who used two different versions of a medium to high-resolution atmospheric general circulation model (MRI-AGCM, Murakami et al. 2012) in an ensemble prescribed with several different sea-surface-temperature (SST) settings. They found TC frequency to decrease (by ~31%) in the Bay of Bengal and increase (by ~46%) in the Arabian Sea. The latter finding is particularly topical as a recent study (Murakami et al. 2017) linked increasing frequency of very intense Arabian Sea TCs in the post-monsoon season with climate change. Another study, Zhang et al. (2019), used medium resolution ensemble

experiments from the NCAR Community Earth System Model (CESM) and predicted tropical depressions in the NIO (and thus likely TCs as well) to increase in the second half of the 21st century.

Murakami et al. (2013) also found a robust reduction of TC genesis frequency in the pre-monsoon season and an increase during the peak-monsoon season. Concerns regarding model dependency of their results were addressed in a follow up study by Murakami et al. (2014). However, in their closing remarks Murakami et al. (2014) indicated that they did not consider the uncertainty introduced by different TC-detection schemes (e.g., Horn et al. 2014) and that model-dependent criteria had been used to tune the detected TC numbers to match the observed TC numbers. They acknowledged that their projection results may be dependent on the TC detection algorithm used, and so indicated that further study may be required to confirm their results using model-independent-detection schemes.

As far as we are aware, this concern has not yet been addressed and is the main motivation behind this paper. The secondary motivation is to examine TC activity more regionally, including analysis and isolation of TC tracks, which to our knowledge have not yet been evaluated for the NIO basin under global warming scenarios. In this paper, multiple climate models from the Coupled Model Intercomparison Project Phase 5 Experiments (CMIP5, Taylor et al. 2012) are used. Given not all these models have the same resolution, we apply a resolution- and model-independent TC detection and tracking scheme (Tory et al. 2013a) called the Okubo-Weiss-Zeta (OWZ). Unlike more traditional detectors, the Tory et al. (2013a) scheme utilizes purely large-scale variables that are resolvable in coarse resolution (CMIP5) data, circumventing detector dependence on resolution. The Tory et al. (2013a) scheme was also independently tuned in ERA-Interim reanalysis data so as to not be model-dependent. Arguably, tuning a detection algorithm elsewhere can impact upon TC projections results, thus elevating the need for a scheme such as Tory et al. (2013a) that can obtain

consistent projection results from climate models with both different resolutions and physical parameterization schemes.

Additionally, we also account for the potential interdependency that exists between certain CMIP5 models (e.g., Knutti et al. 2013). Sanderson et al. (2015) stress how such interdependencies between models can affect multi-model projection results if not properly accounted for, and hence we incorporate this in our model selections and analyses. Model TCs are evaluated over two simulation periods, the "historical climate" over the period 1970-2000 and a climate projection over the period 2070-2100 under high radiative forcing (RCP8.5). An objective TC track cluster analysis (Gaffney et al. 2007) is utilised to provide quantitative regional-scale assessments of TC tracks in models and the historical record.

The outline of this paper is as follows. Section 2 contains data, definitions and methods used in this study. Section 3 evaluates the performance of the OWZ scheme in the NIO using selected CMIP5 models and provides results of projection between the late twentieth- and twenty-first-century climate simulations, also containing relevant discussions with respect to a previous study undertaken in the NIO. Finally, Section 4 provides a summary of the paper.

2 Data, Definitions and Methods

a. Detection and tracking

The OWZ TC detection and tracking algorithm (Tory et al. 2013a) is used in this study to detect and track TCs in all model and reanalysis data without any adjustment of thresholds to accommodate different resolutions. The environmental parameters used at two threshold levels ("initial" and "core") are as follows:

- OWZ [product of absolute vorticity and the Okubo-Weiss parameter (Okubo 1970; Weiss 1991) normalised by the vertical components of relative vorticity squared] at

850 and 500 hPa.

- Relative humidity at 950 and 700 hPa.
- Specific humidity at 950 hPa.
- Vertical wind shear between 850 and 200 hPa.

The algorithm used to trace a TC is summarized below with further details accessible in Tory et al. (2013a) and Bell et al. (2018).

a. Each 1º × 1º grid point is assessed based on the initial threshold values of each parameter at 12-hr intervals.
b. When at least two neighbouring grid points satisfy the initial thresholds of each parameter, these points are considered to represent a single circulation at that point in time.
c. The circulations from step (b) are linked through time by estimating their position in relation to the circulation's expected position based on an averaged 4º × 4º steering wind at 700 hPa.
d. The core thresholds are then applied to each storm track, and if they are satisfied for 48 hrs, a TC is declared.
e. Tracks are terminated when no circulation match is found in the next two time-steps within a generous (~350 km) latitude dependent radius.

The OWZ algorithm has previously undergone scrupulous validation in reanalysis data in terms of annual TC numbers and genesis positions (Tory et al. 2013b), and more recently in terms of tracks (Bell et al. 2018). Crucially, the track validation study of Bell et al. (2018) identified a limitation in the algorithm, suggesting that those TCs lasting less than 2-days after declaration should be discarded for best performance. This study implements this suggestion by removing all such detected TCs in reanalysis and model data. Studies have documented homogeneity issues with short-lived observed TCs due to improvements in

observational capabilities over time in other basins (Landsea et al. 2010). However, we found this impact to be minimal in the NIO basin over the quite recent 1990-2013 period (not shown). For comparison, statistics of observed TCs from the IBTrACS database are shown in Table 1 with and without short-lived TCs removed.

b. TC track definition

The definition of a TC track detected in model and reanalysis data begins from the TC declaration location (i.e., once the core OWZ thresholds have been satisfied for 48 hrs), as this location best matched the timing of a TC first reaching a 10-minute sustained wind speed of 17 m s^{-1} in IBTrACS (see the following section). TCs are terminated when no circulation match is found in the next two time-steps (i.e., the initial thresholds are no longer satisfied).

c. Historical TC records (IBTrACS and ERA-Interim)

The International Best Track Archive for Climate Stewardship – World Meteorological Organization version (IBTrACS-WMO, Knapp et al. 2010a,b) provides a compilation of historical TC data as recorded by meteorological centres and/or forecast agencies that have WMO designation in the surrounding area; in this case the Indian Meteorological Department (IMD). TCs were sourced from this dataset over a 24-year period (1990 to 2013). Tracks are defined to begin at the position a storm reaches a 10-minute sustained wind speed of 17 m s^{-1} (Harper et al. 2010), with those storms not reaching this intensity excluded from the analyses.

TCs detected in ERA-Interim reanalysis data (Dee et al. 2011) are used to provide a second basis of historical TC tracks from the historical record over a 25-year period (1989 to 2013). A second basis of the historical record is required for the NIO due to inconsistencies between TCs in IBTrACS and those detected in model and/or reanalysis data (e.g., Strachan et al. 2013; Tory et al. 2013b,c; Bell et al. 2018; Bell et al. 2020). There are some potential explanations proposed for these inconsistencies being confined to the NIO. These include (1) different forecasting practices and (2) freshwater run off that mixes with the ocean water

from the mountains can affect air-sea heat exchange rates (e.g., Sengupta et al. 2006; Mahadevan et al. 2016). The latter is unlikely to be accounted for in climate model simulations.

d. CMIP5 model data

Thirteen models from the Coupled Model Intercomparison Project (CMIP5, Taylor et al. 2012) are analysed in this study (Table 1). Unlike previous papers (e.g., Bell et al. 2019a,b,c), we have additionally included the MRI-CGCM3 model (Yukimoto et al. 2012) in our analyses. Although prior papers with the OWZ scheme have indicated large overestimations of TC numbers detected with this model (e.g., Tory et al. 2013c; Chand et al. 2017) it was discovered a large percentage of these detections lasted less than 2-days (not shown). Upon removal of these short-lived TCs (as occurs in all other models), a more reasonable TC climatology was produced. This model was also produced by the same institution as the model used in the Murakami et al. papers, whose results we are using as a basis of comparison.

The fifth generation of climate models produced by the CMIP experiments provide a wide array of platforms to assess current and future climate scenarios. The two scenarios assessed in this work include a historical simulation (1970 – 2000) to evaluate and assess climate models' ability to reproduce observed TC climatology, and (2) in the future-climate (2070 – 2100) to determine projected changes as a result of global warming. Future climate CMIP5 simulations are often implemented with one of several Representative Concentration Pathways (RCP, e.g., Van Vuuren 2011) to control the level of carbon emissions in the atmosphere compared to pre-industrial times. In this study, the RCP8.5 scenario that represents a maximum 8.5 W m^{-2} likely increase in radiative forcing over pre-industrial levels (Riahi et al. 2011) was chosen to best elucidate any changing TC behaviour in a warmer climate (e.g., Tory et al. 2013c; Chand et al. 2017).

e. Cluster analysis

The probabilistic curve-clustering (CC) technique of Gaffney et al. (2007) is applied using the CC-Toolbox in MATLAB version 2015a; to group together similar TC tracks in regions of the NIO. The cluster analysis was implemented with each set of TC track data clustered together. Following Camargo et al. (2008) and Nakamura et al. (2017), twenty-five cluster runs were performed with 12 expected maximization (EM) starts with the input order of the tracks being randomized on each run. Linear regression mixture (lrm) models were fitted to each track. The cluster run with the smallest trained log-likelihood value was selected. Four ($k=4$) clusters were used to capture TC track patterns in the NI. This is in contrast with Paliwal and Patwardhan (2013) who used five clusters. We stress the importance of cluster stability and found four clusters, two in each sub-basin to be more stable and better suited for result interpretations.

3 Results and Discussion

a. Preliminary assessment and selection of models

Historical climate TC tracks detected by the OWZ algorithm in each of the 13 CMIP5 models, as well as those detected in ERA-Interim reanalysis data and observed in IBTrACS, are shown in Fig. 2. Note that hereafter IBTrACS and ERA-Interim TCs are collectively referred to as the "historical records" for the reasons highlighted in Section 2c. Some discrepancies between TCs in the historical records and model simulations were noted. In particular, most models show increased genesis equatorward of 10°N in the Bay of Bengal and 5°N in the Arabian Sea. Similarly, there was a failure in detecting higher latitude TCs in the Arabian Sea in some models (e.g., CSIROmk3.6, HadGEM2-ES and the ACCESS models). It also appears some TCs detected in CSIRO-Mk3.6 track towards the equator in the northern Bay of Bengal (Fig. 2).

Before analysis of projections is attempted, it is important to carefully select models that best represent the TC characteristics to be analysed in the historical records while ensuring models are independent of each other (see Knutti et al. 2013; Sanderson et al. 2015). The aim here is to provide early season, peak monsoon and late season projections as well as projections for the Arabian Sea and Bay of Bengal; thus the models are examined on their performance accordingly (Table 1). It should also be emphasised that there is no attempt made to correct the weighting of models in the multi-model mean constructions, hence models with the most simulated TCs have a slightly stronger weighting within the multi-model means. This disqualifies models with very high (MIROC5) and very low (CNRM-CM5) TC detections from being included in multi-model means. However, if these models were to perform well in other characteristics, they may be included in results separate from a multi-model mean (as seen later with MIROC5).

Based on the model independence analyses of Knutti et al. (2013), who analysed similarities between models in control states and response to RCP8.5, the following models in the three subgroups (HAD-ACC, GFDL and BCC) can be considered dependent:

- HAD-ACC: HadGEM2-ES, ACCESS1.0 and ACCESS1.3.
- GFDL: GFDL-ESM2M, GFDL-CM3 and GFDL-ESM2G.
- BCC: BCC-CSM1.1 and BCC-CSM1.1m.

This leaves CCSM4, MIROC5, CNRM-CM5, CSIROMk3.7 and MRI-CGCM3 as the remaining independent models. By combining this independence information with model skill assessments in Table 1, a group of 4 models was systematically decided upon to form a four-model mean (4-M). BCC-CSM1.1M was the best performing model, followed by MRI-CGCM3, ACCESS1.3 and GFDL-ESM2G. Note that the latter three models all performed poorly in simulating the ratios between early and late season TCs while MIROC5 best

performed in this metric outside of the two BCC models. Almost all models overestimated TCs during peak monsoon season compared with the early season (pre-monsoon) although early season TCs were severely underestimated in all models except MIROC5. In contrast, when comparing the peak-monsoon season to just the post-monsoon TCs, a suppression of TC numbers during peak monsoon season was simulated by most models.

b. Projection of TC numbers

Projection results (Table 2) from the best performing model, 4-M and an additional 6-M mean (see caption of Table 2) under RCP8.5 show increased TC numbers in the Arabian Sea (30–64%) and decreased TC numbers in the Bay of Bengal (22–43%), consistent with Murakami et al. (2013). The NIO as a whole was projected to decrease by 8–14%, with early season (pre-monsoon) TCs decreasing by 29–36% and late season (post-monsoon) TCs increasing by 5–27% (Table 3). With exception of the peak monsoon season ([-22 – 64%]), projection results from each of the best, 4-M and 6-M models all agreed on the sign of change under the RCP8.5 warming condition (Tables 2 and 3). Results for peak-monsoon and post-monsoon season projections differ to the findings of Murakami et al. (2013), who found an increase in the peak-monsoon season and no change in post-monsoon TC frequencies. We do note that Murakami et al. (2013) only used the more active months of October and November to define the post-monsoon while OND was used in this study. This small discrepancy is unlikely to impact on conclusions.

c. Cluster analysis of TC tracks

i. Historical simulations

Cluster analysis is applied to TC tracks from different sources (IBTrACS, ERA-Interim and CMIP5) simultaneously. Four clusters (i.e., k=4) were used to describe TC tracks in the NIO, two in the Arabian Sea and two in the Bay of Bengal. An additional cluster to the three used for the NIO basin in Bell et al. (2018) is introduced so that model overestimations of Arabian

Sea TC detections toward the equator can be isolated (AS1, Fig. 3; Table 4). It was found that the inclusion of IBTrACS TCs in the clustering analysis led to spurious results (Fig. 3a), therefore a subsequent cluster analysis was performed without the IBTrACS TCs (Fig. 3b). This appears to correct the previous errors, as we see a much closer match between the RCP8.5 (orange) and historical (blue) mean genesis positions and trajectories. Results of the secondary cluster analysis (Fig. 3b) are used throughout the remainder of this paper.

ii. RCP8.5 projections

The earlier finding of a projected increase (decrease) in Arabian Sea (Bay of Bengal) annual TC numbers are further stratified by track cluster analysis, splitting each sub-region into two distinct groups of tracks (Table 4). Noting TCs belonging to the AS1 cluster were not as readily found in the historical records as they are detected in models. However, the overall projection result does not seem to be dependent on the AS1 cluster, as projected increases in both Arabian Sea clusters are similar (26% and 29% respectively). Likewise, both Bay of Bengal clusters also undergo a similar projected frequency decrease (29% and 25% respectively).

Our earlier finding of projected decreases (increases) in early (late) season TC numbers were also further stratified by clusters (Table 5). Failure of each 4-M member to correctly simulate monsoonal variations in TC frequency (Table 1) casts doubt onto some of these projection results. For early season TCs, a statistically robust projected decrease in the two Bay of Bengal clusters was partially offset by a robust increase in the northern Arabian Sea (AS2). For late season TCs, results were not found to be as robust as the early season. The decrease in the southern Bay of Bengal (BoB1) was the least robust, biased by a 50% reduction in TCs from the ACCESS1.3 model (not shown). The remaining three clusters in the late season were projected to increase, with three of four models agreeing on the sign of change (Table 5).

iii. Projected changes in large-scale environmental conditions

Prior studies (e.g., Pattanaik 2005; Chan 2007; Ng and Chan 2012) have concluded that variations in TC activity in and around the NIO are due to variations in the large-scale atmospheric circulation, rather than SST. Historically, emphasis has been placed on vertical wind shear in the Bay of Bengal (Xavier and Joseph 2000) and relative humidity in the Arabian Sea (Evan and Camargo 2011). Ng and Chan (2012) attributed wind shear, humidity and geopotential energy, among other conditions, to variability in in the Bay of Bengal during the late season (OND) but did not find causes of variability during the early season (AMJ).

Here we analyse the change in three relevant large-scale parameters between the RCP8.5 and historical model simulations during the early (AMJ) and late (OND) seasons (Fig. 4). Projected changes in relative humidity and vertical wind shear during AMJ are consistent with a projected increase of TC activity in the northern Arabian Sea (AS2). Reductions of AMJ TC activity over the Bay of Bengal are consistent with changes in vertical ascent (omega). A sharper decrease in TC frequency in the Southern portion of the Bay (BoB1, Table 5) appears to be consistent with changes to relative humidity and vertical ascent rather than vertical wind shear. For the OND months, where projection results were more variable, relative humidity underwent a significant increase and appears to be the most consistent with projected changes in TC frequency (where all clusters except for BoB1 were likely to increase). Changes in the favourability of vertical ascent were very similar to the pattern of relative humidity. In contrast, vertical wind shear was reduced over the southern regions, particularly in the Bay of Bengal (BoB1). However we note that changes in vertical wind shear over the Bay of Bengal were not considered significant in terms of model agreement (Fig. 4).

4. TC track density change

Here we account for both TC frequency and track characteristics by measuring TC track density. This is measured by counting the number of individual TCs entering 2.5 x 2.5° grid boxes over the entire NIO (30°–100°E). Note certain terminology differences between this study and Murakami et al. (2013) where TC track density is simply referred to as TC frequency or "TCF".

TC track densities were computed for the RCP8.5 and historical climate model simulations. Resulting historical densities were then subtracted from RCP8.5 densities (Fig. 5a) to highlight projected changes. Inclusive of each cluster in the NIO, TC track density was found to increase (decrease) over the Arabian Sea (Bay of Bengal), consistent with earlier findings related to TC frequency (Section 3b). In some grid boxes, particularly the Arabian Sea, all four models in the 4-M mean agreed on the sign of change under RCP8.5 (yellow boxes, Fig. 5b). We note a remarkable similarity between this figure and regions considered significant in Murakami et al. (2013, their Fig. 5a).

Next, in order to isolate changes in TC track directions, the number of TCs in each cluster between the historical and RCP8.5 climate model simulations were held fixed to compute normalised TC track densities in each cluster. Resulting track densities from the historical simulation were then subtracted from the RCP8.5 model track densities (Fig. 5c-f). This isolates non-frequency related changes for each cluster. Projections of normalised track density under RCP8.5 was quite similar to the historical simulation for AS1, AS2 and BoB2. However, BoB1 showed a marked difference in normalised track density under the RCP8.5 scenario (Fig. 5e). It appears BoB1 TCs are shifted poleward (consistent with Fig. 3b) and are more likely to make a crossing through southern India (rather than Sri Lanka) into the Arabian Sea, further increasing overall TC track density in the Arabian Sea (Fig. 5a).

A caveat of the above result is that two models in the 4-M mean had historical TC

detection biases equatorward of 5°N in the Arabian Sea. In the RCP8.5 simulation, TCs were not detected here (not shown); reducing confidence in the poleward shift found for BoB1. We also note that BCC-CSM1.1m projected an equatorward shift in genesis position in contrast to the other three models comprising the 4-M.

a. TC landfall projections

Impacts to TC landfall rates are deduced from prior analyses. From Fig. 5a, it appears the eastern coast of India (inclusive of Bangladesh) all the way down to Sri Lanka may experience a decrease in TC landfall rates (up to 2 per decade) mainly due to decreasing TC numbers in the Bay of Bengal. Notably, differences in landfall rates become marginal along the eastern coast of India between 9–14°N, likely due to a somewhat spurious poleward shift of BoB1 cluster TCs in the RCP8.5 scenario (Fig. 5e).

For the western coast of India, landfall events are projected to remain rare occurrences, as TCs in the Arabian sea continue to track westward. However, BoB1 TCs were projected to increase in density on the western coast after crossing from the east (Fig. 5e), although this had little effect on the overall density (Fig. 5a). The surrounding landscape to the west in the Arabian Sea (e.g., African and Middle eastern countries) see only a small increase in landfall events (~0.5 TCs per decade), despite large percentage increases in TC frequency.

5. Summary and Discussion

Projection results in the NIO TC basin were complicated by a mismatch between TCs detected in models and those recorded in IBTrACS, as found in several other studies, including those that used a different TC detection and tracking scheme. Murakami et al. (2013) found an increase (decrease) of TC genesis frequency in the Arabian Sea (Bay of Bengal) through their model simulation of a carbon forced environment. In a subsequent

study those authors addressed issues of model-dependency but also raised concerns about TC detection scheme dependence and its possible impacts on results; noting that no model or detector is perfect and that different detectors can produce different results when applied to the same model (Horn et al. 2014). A model-independent TC detection scheme (Tory et al. 2013a) was used in the present study to address such concerns, and to also produce regional-scale TC track projections for the NIO.

Projected changes in NIO TCs were determined between historical climate conditions (1970-2000) and projected climate conditions (2070-2100) under the RCP8.5 warming scenario. Intraseasonal effects of early season (pre-monsoon), peak monsoon and late season (post-monsoon) were also analysed. The bulk of the analysis utilised a multi-model mean comprised of four independent CMIP5 models (4-M). All TC tracks under analysis were input to the clustering algorithm simultaneously. Removal of IBTrACS TCs from the clustering analysis improved interpretation and consistency. Four clusters were used, two in the Arabian Sea, and two in the Bay of Bengal, noting TCs in the southernmost Arabian Sea cluster were overestimated by most models.

The main results of this study are summarised as follows.

- In the future climate projection, consistent with Murakami et al. (2013), TC genesis frequency was found to be significantly suppressed in the Bay of Bengal and significantly enhanced in the Arabian Sea.

- TC genesis frequency was found to be significantly decreased during the pre-monsoon season. Different to Murakami et al. (2013), TC genesis frequency was found to be increased during the post-monsoon season in each region except the southern Bay of Bengal (BoB1). Although we note our latter changes cannot be considered statistically significant as only three out of the four models tested agreed on the sign of change. Also in contrast with Murakami et al. (2013) were projections

of peak monsoon season TC genesis frequency, where we projected a decrease in the northern Bay of Bengal (BoB2).

- Increased TC genesis in the post-monsoon season in the northern Bay of Bengal (BoB2) was consistent with changes in relative humidity and vertical ascent. Similarly, pre-monsoon season TC genesis frequency in the northern Arabian Sea (AS2) was also increased but was instead consistent with changes in relative humidity and vertical wind shear.

- Despite these changes, the northern Bay of Bengal (BoB2) remained the most active TC development region under the RCP8.5 scenario and the southern Arabian Sea (AS1) the least active.

- TC track density change included a decrease of up to 2 TCs per decade impacting the eastern coast of India and a small increase (up to 0.5 TCs per decade) hitting Eastern Africa, Oman and Yemen; consistent with projected changes in TC genesis. A possible poleward shift in southern Bay of Bengal TCs (BoB1) that track west into the Arabian Sea was noted, resulting in only a marginal decrease of landfall activity between 9–14°N along the east Indian coastline. However, the latter result was complicated by the presence of equatorward TC detection biases in the historical model simulations. These biases were found in the RCP8.5 projections in two of the four independent models used.

In closing, we note a genuine similarity between overall projection results in this paper and Murakami et al. (2013). Although, at finer scales some inconsistencies were noted between the studies, and between some models examined here, especially concerning intra-seasonal TC activity projections. Further increases in the robustness of TC projections in the NIO can be achieved as simulation of the Asian monsoon improves in climate models.

References

Alam MM, Hossain MA, Shafee S. 2003. Frequency of Bay of Bengal cyclonic storms and depressions crossing different coastal zones. *International Journal of Climatology* **23**, 1119–1125.

Bell SS, Chand SS, Tory KJ, Turville, C. 2018. Statistical assessment of the OWZ tropical cyclone tracking scheme in ERA-Interim. *Journal of Climate*, **31**, 2217–2232.

Bell SS, Chand SS, Tory KJ, Dowdy AJ, Turville C, Ye, H. 2019a. Projections of Southern Hemisphere Tropical Cyclone Track Density using CMIP5 models. *Climate Dynamics*, **52**, 6065-6079. doi:10.1007/s00382-018-4497-4

Bell SS, Chand SS, Tory KJ, and Turville C, Ye H. 2019b. Eastern North Pacific tropical cyclone activity in historical and future CMIP5 experiments: assessment with a model-independent tracking scheme. *Climate Dynamics,* https://doi.org/10.1007/s00382-019-04830-0

Bell SS, Chand SS, Camargo, SJ, Tory KJ, Turville C, Ye H. 2019c. Western North Pacific tropical cyclone tracks in CMIP5 models: Assessment using a model-independent detection and tracking scheme. *Journal of Climate,* https://doi.org/10.1175/JCLI-D-18-0785.1

Bell SS, Chand SS, Turville C. 2020. Projected changes in ENSO-driven regional tropical cyclone tracks. *Climate Dynamics.,* **54**, 2533-2559.

Bi. D., and Coauthors, 2012. The ACCESS Coupled Model: Description, Control Climate and Evaluation. *Australian Meteorology and Oceanography Journal*, CMIP5 Special Issue, **63**, 41–64.

Camargo SJ, Robertson AW, Barnston AG, Ghil M. 2008. Clustering of eastern North Pacific tropical cyclone tracks: ENSO and MJO effects. *Geochemistry, Geophysics, Geosystems*, **9**, Q06V05, doi:10.1029/2007GC001861.

Chan JCL. 2007. Interannual variations of intense typhoon activity. *Tellus*, **59A**, 455–460.

Chand SS, Tory KJ, Ye H, Walsh KJE. 2017. Projected increase in El Niño-driven tropical cyclone frequency in the Pacific. *Nature Climate Change*. **7**, 123–127, doi:10.1038/nclimate3181

Collier MA and Coauthors, 2011. The CSIRO-Mk3.6.0 Atmosphere-Ocean GCM: participation in CMIP5 and data publication. In: 19th International Congress on Modelling and Simulation, Perth, Australia, 12–16 December 2011 http://mssanz.org.au/modsim2011

Dee DP and Coauthors, 2011. The ERA-Interim reanalysis: configuration and performance of the data assimilation system. *Quarterly Journal of the Royal Meteorological Soc*iety, **137**, 553–597, doi:10.1002/qj.828

Donner LJ and Coauthors, 2011. The dynamical core, physical parameterizations, and basic simulation characteristics of the atmospheric component AM3 of the GFDL global coupled model CM3. *Journal of Climate*, **24**, 3484–3519, doi:10.1175/2011JCLI3955.1.

Emanuel K. 2005. The Great East Pakistan Cyclone of November 1970. In: Divine Wind. 221–225.

Evan AT, Camargo SJ. 2011. A Climatology of Arabian Sea Cyclonic Storms. *Journal of Climate*, **24**, 140–158, https://doi.org/10.1175/2010JCLI3611.1

Gaffney SJ, Robertson AW, Smyth P, Camargo SJ, Ghil M. 2007. Probabilistic clustering of extratropical cyclones using regression mixture models. *Climate Dynamics*, **29**, 423–440.

Gent PR and Coauthors 2011. The community climate system model version 4. *Journal of Climate Special Collections,* **24,** 4973–4991.

Harper BA, Kepert JD, Ginger JD. 2010. Guidelines for converting between various wind averaging periods in tropical cyclone conditions. *World Meteorological Organization Technical Document*. 1555, 64 pp., https://www.wmo.int/pages/prog/www/tcp/documents/WMO_TD_1555_en.pdf.

Horn M and Coauthors 2014. Tracking scheme dependence of simulated tropical cyclone response to idealized climate simulations. *Journal of Climate*, **27**, 9197–9213, https://doi.org/10.1175/JCLI-D-14-00200.1.

Jones CD 2011. The HadGEM2-ES implementation of CMIP5 centennial simulations. *Geoscientific Model Development,* **4**, 543–570.

Knapp KR, Kruk MC, Levinson DH, Diamond HJ, Neumann CJ. 2010a. The International Best Track Archive for Climate Stewardship (IBTrACS) unifying tropical cyclone data. *Bulletin of the American Meteorological Society*, **91**, 363–376, https://doi.org/10.1175/2009BAMS2755.1.

Knapp KR, Appleguist S, Diamond HJ, Kossin JP, Kruk M, Schreck C. 2010b. NCDC International Best Track Archive for Climate Stewardship (IBTrACS) Project, version 3. NOAA National Centers for Environmental Information. Subset used: January 1989–December 2013, accessed 12 August 2016, https://doi.org/10.7289/V5NK3BZP.

Knutti R, Masson D, Gettelman A. 2013. Climate model genealogy: Generation CMIP5 and how we got there. *Geophys. Res. Lett.* **40**, 1194-1199

Landsea CW, Vecchi GA, Bengtsson L, Knutson TR. 2010. Impact of Duration Thresholds on Atlantic Tropical Cyclone Counts. *Journal of Climate*, **23**, 2508–2519.

Lee T. 2009. Eiffient Bivariate KDE (2Dim) (https://www.mathworks.com/matlabcentral/fileexchange/22999-eiffient-bivariate-kde-2dim), MATLAB Central File Exchange. Retrieved February 1, 2015.

Mahadevan AG, Jaeger S, Freillich M, Omand MM, Shroyer EL, Sengupta D. 2016. Freshwater in the Bay of Bengal: Its Fate and Role in Air-Sea Heat Exchange. *Oceanography Society*, **29**, 72–81.

Mohapatra M, Bandyopadhyay BK, Tyagi A. 2014. Status and plans for operational tropical cyclone forecasting and warning systems in the North Indian Ocean region. *In: Mohanty UC, Mohapatra M, Singh OP, Bandyopadhyay BK, Rathore LS (eds) Monitoring and prediction of tropical cyclones in the Indian Ocean and Climate Change.*

Murakami H and Coauthors 2012. Future changes in tropical cyclone activity projected by the new high-resolution MRI-AGCM. *Journal of Climate*, **25**, 3237–3260, doi:10.1175/JCLI-D-11-00415.1.

Murakami H, Sugi M, Kitoh A. 2013. Future changes in tropical cyclone activity in the North Indian Ocean projected by high-resolution MRI-AGCMs. *Climate. Dyn*amics, **40**, 1949–1968, https://doi.org/10.1007/s00382-012-1407-z

Murakami H, Vecchi GA, Underwood S. 2017. Increasing frequency of extremely severe cyclonic storms over the Arabian Sea. *Nature Climate Change*, **7**, 885–889,

https://doi.org/10.1038/s41558-017-0008-6

Murakami H, Hsu PC, Arakawa O, Li T. 2014. Influence of Model Biases on Projected Future Changes in Tropical Cyclone Frequency of Occurrence. *Journal of Climate*, **27**, 2159-2181, doi:10.1175/JCLI-D-13-00436.1

Nakamura J and Coauthors 2017. Western North Pacific Tropical Cyclone Model Tracks in Present and Future Climates. *Journal of Geophysical Research: Atmospheres*, **122**, 1333–1361, doi:0.1175/JCLI-D-13-00646.1.

Ng EK, Chan JCL. 2012. Interannual variations of tropical cyclone activity over the north Indian Ocean. *International Journal of Climatology,* **32**, 819-830. doi:10.1002/joc.2304

Okubo A, 1970. Horizontal dispersion of floatable particles in the vicinity of velocity singularities such as convergences. *Deep-Sea Research,* **17**, 445–454.

Paliwal M, Patwardhan A. 2013. Identification of clusters in tropical cyclone tracks of North Indian Ocean. *Natural Hazards*, **68**, 645–656.

Pattanaik DR. 2005. Variability of oceanic and atmospheric conditions during active and inactive periods of storms over the Indian region. *International Journal of Climatology,* **25**, 1523– 1530.

Riahi K, Rao S, Krey V, Cho C, Chirkov V, Fischer G, Kindermann G, Nakicenovic N, Rafai P. 2011. RCP 8.5—A scenario of comparatively high greenhouse gas emissions. *Climatic Change,* **109**, 33-57, doi:10.1007/s10584-011-0149-y

Sanderson B, Knutti R, Caldwell P. 2015. A Representative Democracy to Reduce Interdependency in a Multimodel Ensemble. *Journal of Climate*, **28**, 5171–5194.

Sattar AM, Cheung KKW. 2019. Comparison between the active tropical cyclone seasons over the Arabian Sea and Bay of Bengal. *International Journal of Climatology*. **39**, 5486–5502, https://doi.org/10.1002/joc.6167

Sengupta D, Bharath Raj GN, Shenoi SSC. 2006. Surface freshwater from Bay of Bengal runoff and Indonesian Throughflow in the tropical Indian Ocean. *Geophysical Research Letters,* **33**, L22609, doi:10.1029/2006GL027573.

Singh OP, Ali Khan TM, Rahman MdS. 2000. Changes in the frequency of tropical cyclones over the North Indian Ocean, *Meteorology and Atmospheric Physics,* **75**, 11–12.

Strachan JP, Vidale PL, Hodges K, Roberts M, Demory ME. 2013. Investigating global tropical cyclone activity with a hierarchy of AGCMs: The role of model resolution. *Journal of Climate,* **26**, 133–152, https://doi.org/10.1175/JCLI-D-12-00012.1.

Taylor KE, Stouffer RJ, Meehl GA. 2012. An overview of CMIP5 and the experiment design. *Bulletin of the American Meteorological Society*, **93**, 485–498.

Tory KJ, Dare RA, Davidson NE, McBride JL, Chand SS. 2013a. The importance of low-deformation vorticity in tropical cyclone formation. *Atmospheric Chemistry and Physics,* **13**, 2115–2132.

Tory KJ, Chand SS, Dare RA, McBride JL. 2013b. The development and assessment of a model-, grid-, and basin independent tropical cyclone detection scheme. *Journal of Climate,* **26**, 5493–5507, https://doi.org/10.1175/JCLI-D-12-00510.1.

Tory KJ, Chand SS, McBride JL, Ye H, Dare RA. 2013c. Projected changes in late-twenty-first century tropical cyclone frequency in 13 coupled climate models from the Coupled Model Intercomparison Project Phase 5. *Journal of Climate*, **26**, 9946–9959.

Van Vuuren DP and Coauthors 2011. The representative concentration pathways: an overview. *Climatic Change*, **109**, 5-31, DOI:10.1007/s10584-011-0148-z

Voldoire A and Coauthors 2012. The CNRM-CM5.1 global climate model: description and basic evaluation. *Climate Dynamics*, **40**, 2091-2121

Watanabe M, and Coauthors 2010. Improved climate simulation by MIROC5: Mean states, variability, and climate sensitivity. *Journal of Climate*, **23**, 6312–6335, doi:10.1175/2010JCLI3679.1.

Weiss J. 1991. The dynamics of enstrophy transfer in two-dimensional hydrodynamics. *Physica D*, **48**, 273–294.

Wu T, and Coauthors, 2014. An overview of BCC climate system model development and application for climate change studies. *Journal of Meteorological Research.*, **28,** 34–56, doi:10.1007/s13351-014-3041-7.

Xavier PK, Joseph PV. 2000. Vertical wind shear in relation to frequency of monsoon depressions and tropical cyclones of Indian Seas. Proc. TROPMET-2000, National Symp. On Ocean and Atmosphere, Cochin, India, *Indian Meteorological Society*, 232– 245.

Yukimoto S, and Coauthors 2012. A New Global Climate Model of the Meteorological Research Institute: MRI-CGCM3. *Journal of Meterological. Society. Japan*, **90A,** 23–64.

Zhang W, Vittal H, Villarini G. 2019. Potential Impacts of Anthropogenic Forcing on the Frequency of Tropical Depressions in the North Indian Ocean in 2018. *Journal of Marines Science and Engineering*, **7**, https://doi.org/10.3390/jmse7120436

	Arabian Sea	Bay of Bengal	Ratio AS/BoB	Early (E)	Peak (P)	Late (L)	Ratio E/L	Ratio P/(E+L)	Peak Min	Total (p/yr)	Reference
IBTrACS	1.6	4.6	0.35	2.0	1.5	2.5	0.79	0.34	Y	6.2	Knapp et al. 2010a,b
IBTrACS (>2day)	1.1	3.0	0.37	1.5	0.7	2.5	0.62	0.18	Y	5.1	-
ERA-Interim	1.4	3.3	0.42	1.5	0.7	2.4	0.62	0.18	Y	4.7	Dee et al. 2011
CSIROmk3.6+	0.5	4.0	**0.14**	0.8	1.0	2.7	**0.30**	0.29	N	4.6	Collier et al. 2011
CNRM-CM5	0.2	0.6	0.28	0.1	0.0	0.6	**0.11**	**0.00**	Y	**0.7**	**Voldoire et al. 2012**
GFDL-2m	1.2	3.4	0.34	0.4	1.6	2.1	**0.20**	**0.63**	N	4.6	Donner et al. 2011
CCSM4+	1.9	2.7	**0.69**	0.5	1.1	2.5	**0.19**	0.36	N	4.6	Gent et al. 2011
GFDLCM3	1.7	2.8	**0.60**	0.5	0.9	2.9	**0.15**	0.26	N	4.5	Donner et al. 2011
ACCESS1.0	0.5	3.5	**0.16**	0.3	1.6	1.7	**0.19**	**0.78**	N	4.0	Bi et al. 2012
BCC_CSM1.1	0.3	0.8	0.31	0.3	0.4	0.4	0.75	**0.62**	N	**1.1**	Wu et al. 2014
MIROC5	2.2	6.9	0.31	2.8	2.4	3.5	0.81	0.37	Y	**9.1**	Watanabe et al. 2010
GFDL-2G*	1.2	4.0	0.29	0.9	1.4	2.5	**0.35**	**0.42**	N	5.2	Donner et al. 2011
HADGEM2	0.3	3.5	**0.09**	0.5	1.5	1.5	**0.30**	**0.77**	N	3.8	Jones et al. 2011
ACCESS1.3*	1.3	3.4	0.38	0.1	0.7	3.4	**0.02**	0.21	N	4.6	Bi et al. 2012
BCC-1.1m*	1.0	2.3	0.43	0.8	1.0	1.4	0.57	**0.46**	N	3.3	Wu et al. 2014
MRI-CGC*	1.7	3.6	0.48	0.7	2.0	2.5	**0.27**	**0.64**	N	5.3	Yukimoto et al. 2012

Table 1: Climate averages of the number of TC occurrences (per year) in several regions and temporal periods within and over the NIO TC basin. Model values in bold indicate sufficient deviation from the historical record values. Models with an asterisk (*) are members of the 4-model mean (4-M), those with a plus (+) are used in the 6-M.

	hist			RCP8.5			Change (%)		
	AS	**BoB**	**Total**	**AS**	**BoB**	**Total**	**AS**	**BoB**	**Total**
Best	1.0	2.3	3.3	1.6	1.3	3.0	+64	-43	-10
4-M	1.3	3.3	4.6	1.7	2.6	4.3	+36	-22	-8
6-M	1.3	3.3	4.6	1.7	2.5	4.2	+30	-25	-14

Table 2: Projection results of TC frequencies (per year) in the Arabian Sea (AS) and Bay of Bengal (BoB) and combined (Total), for the best forming model (BCC-CSM1.1M), independent best performing model mean (4-M) and the latter with the inclusion of two additional models CSIROMK3.6 and CCSM4 (6-M).

	hist			RCP8.5			Change (%)		
	Early	**Peak**	**Late**	**Early**	**Peak**	**Late**	**Early**	**Peak**	**Late**
BCC1.1m	0.8	1.0	1.4	0.5	0.8	1.6	-29	-22	+27
MIROC5	2.8	2.4	3.5	2.0	3.9	4.4	-32	+64	+14
4-M	0.6	1.3	2.5	0.4	1.0	2.6	-36	-22	+5
6-M	0.6	1.2	2.5	0.4	1.1	2.7	-35	-11	+8

Table 3: Projection results for early season (April-June), peak monsoon season (July-September) and late season (October-December) TC frequencies (per year). The early/late season ratio of TC numbers in the historically simulated BCC-CSM1.1M and MIROC5 models were the best match to the ratios in observed and reanalysis data. MIROC5 was the only model to meet both peak season criteria (Table 1).

	ERA-Int	Hist	RCP8.5	P (%)	SA
AS1	0.2	0.9	1.2	+26	3/4
AS2	1.6	0.5	0.7	**+29**	**4/4**
BoB1	1.0	1.4	1.0	**-29**	**4/4**
BoB2	2.0	1.8	1.3	**-25**	**4/4**

Table 4: Composition of TC frequency (per year) within TC track clusters and projected change under RCP8.5 (P). Sign agreement (SA) on the projected change between the four models of the 4-M, bolding represents >95% significance.

	ERA-I	Hist	RCP8.5	P (%)	SA
Early					
AS1	0	0	0	-	-
AS2	0.5	0.2	0.4	**+71**	**3/3**
BoB1	0.1	0.6	0.1	**-84**	**4/4**
BoB2	0.7	1.6	1.1	**-49**	**3/3**
Peak					
AS1	0.0	0.1	0.2	+200	1/1
AS2	0.2	0.8	1.0	+25	3/4
BoB1	0.0	0.3	0.3	-	1/2
BoB2	0.4	4.1	2.6	**-35**	**4/4**
Late					
AS1	0.2	3.5	4.1	+19	3/4
AS2	0.6	1.0	1.3	+22	3/4
BoB1	0.6	4.0	3.4	-15	2/4
BoB2	0.6	1.4	1.6	+17	3/4

Table 5: Composition of early season (April-June), peak monsoon (July- September) and late season (October-December) TC frequency (per year) within TC track clusters and projected change under RCP8.5 (P). Sign agreement (SA) on the projected change between the four models of the 4-M where bolding represents >95% significance. In some cases, models had the same number of TC detections in the historical and RCP8.5 simulations or had no TC detections in either. These were excluded from SA consideration.

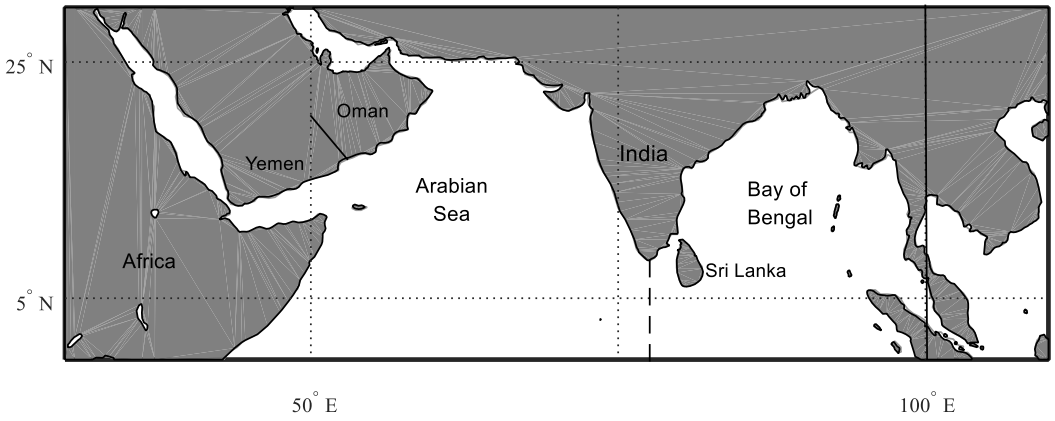

Fig. 1: The North Indian Ocean TC basin (30-100°E). Note TCs forming west of 77.5°E are referred to as Arabian Sea storms, and those forming east of 77.5°E are referred to as Bay of Bengal storms.

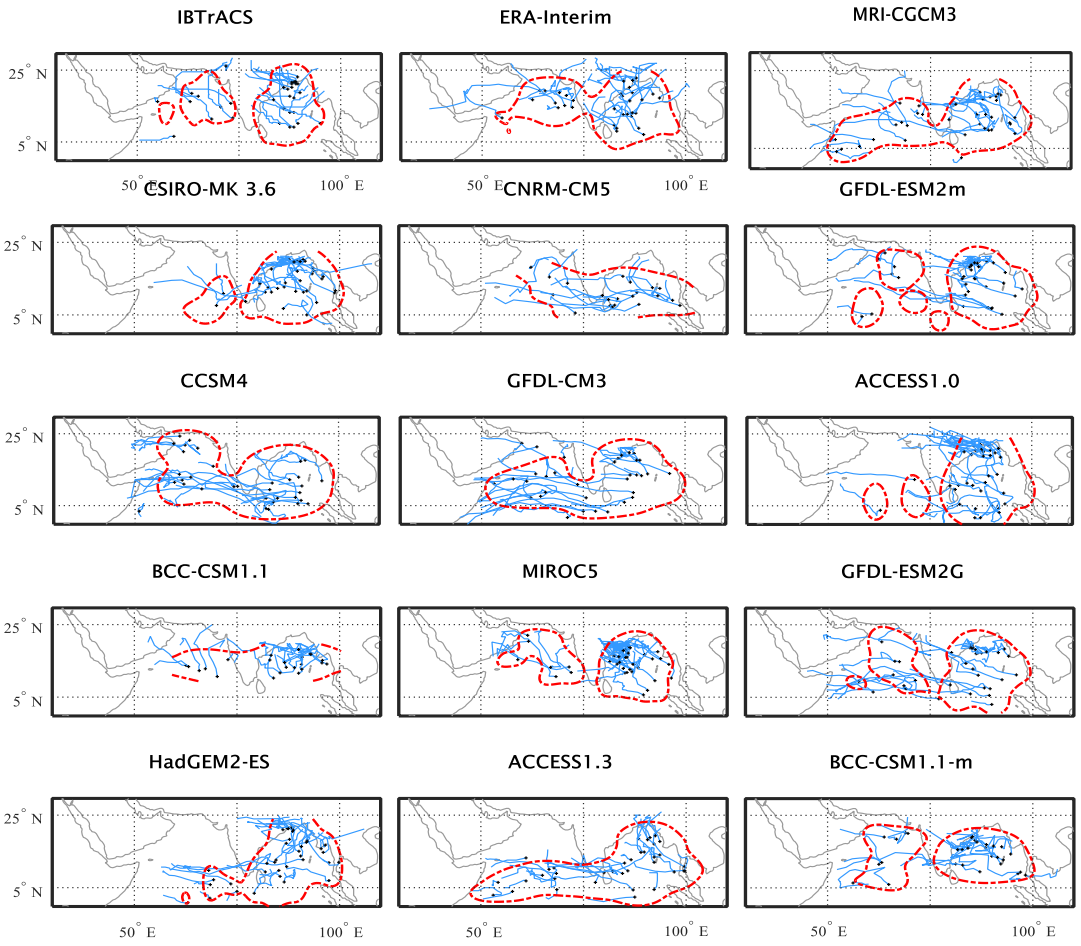

Fig. 2: TC genesis locations (black +'s) and tracks (blue lines) from IBTrACS observations (1990-2013), ERA-Interim reanalysis (1989-2013) and CMIP5 historical model simulations (1970-2000). A random sample of up to 40 TC tracks are shown in each panel. Density estimates based on a kernel function (Lee 2009) enclose approximately 75% of TC genesis (red contours).

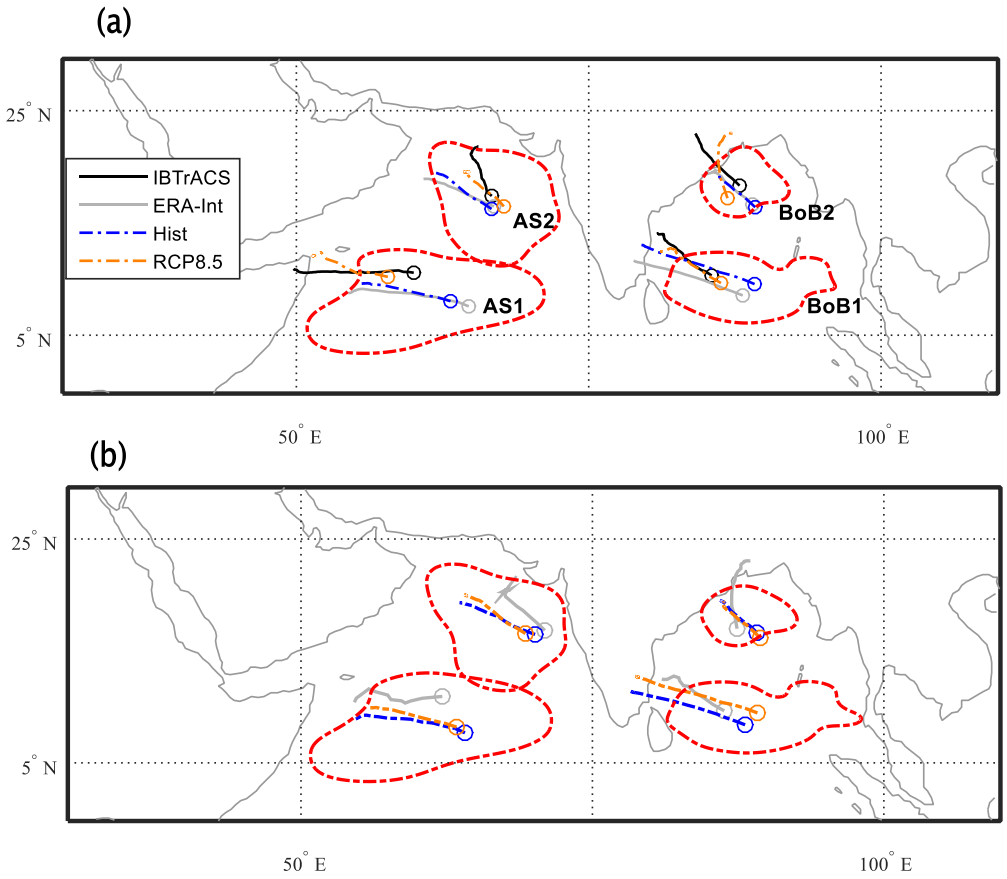

Fig. 3: Decomposed cluster mean track trajectories from (a) the original cluster analysis and (b) a subsequent cluster analysis (where IBTrACS TCs were excluded). Cluster names are retained between both analyses, with two in the Arabian Sea (AS) and two in the Bay of Bengal (BoB). Kernel density estimates (Lee 2009) enclose 50% of genesis positions in each cluster.

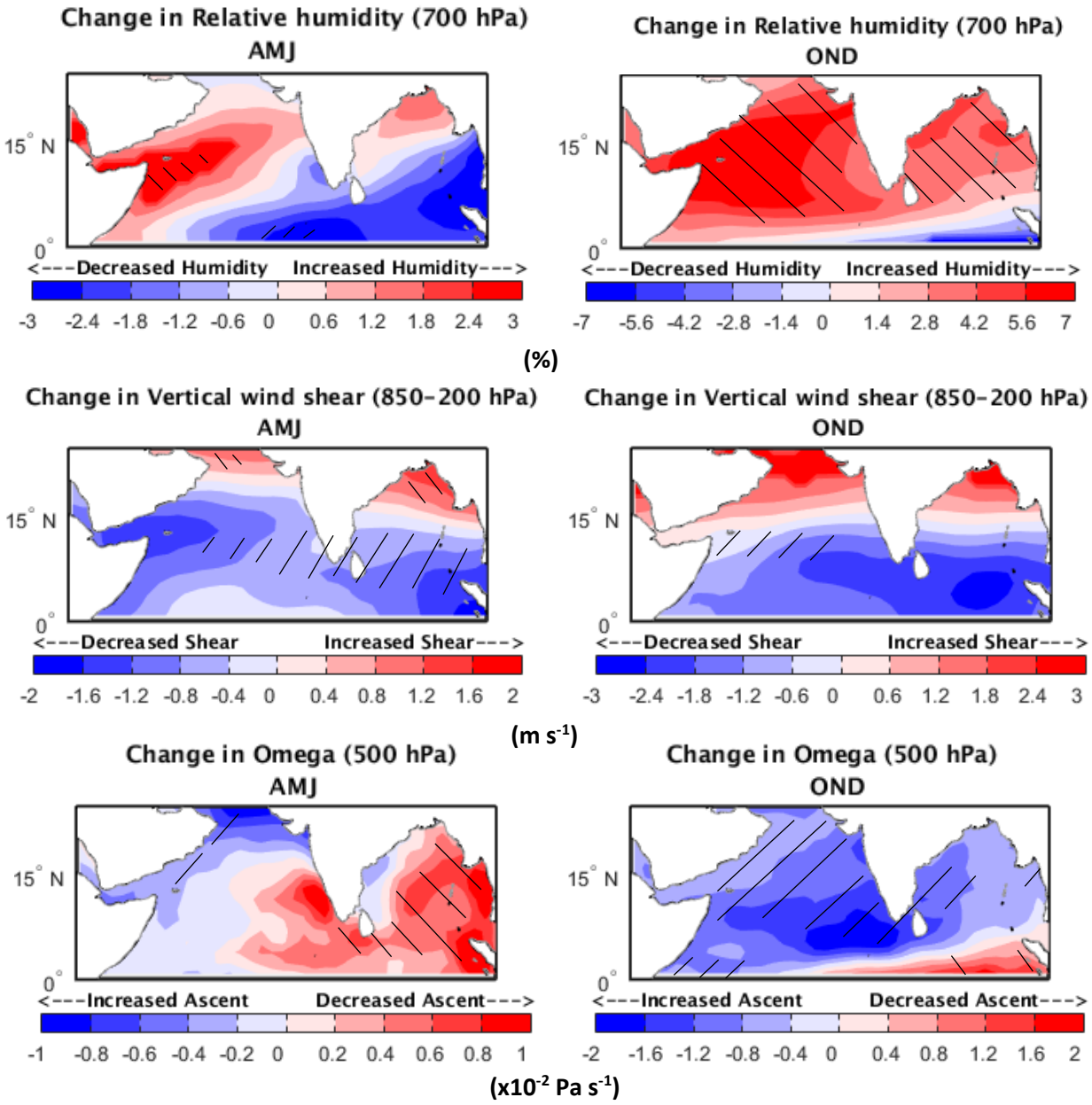

Fig. 4: Difference in the kernel densities of large-scale TC genesis parameters between RCP8.5 and historical conditions during pre-monsoon (AMJ) and post-monsoon (OND) seasons. Results were averaged over five models, those used in the 4-M and MIROC5. Stippling indicates all five models agreed on the sign of change.

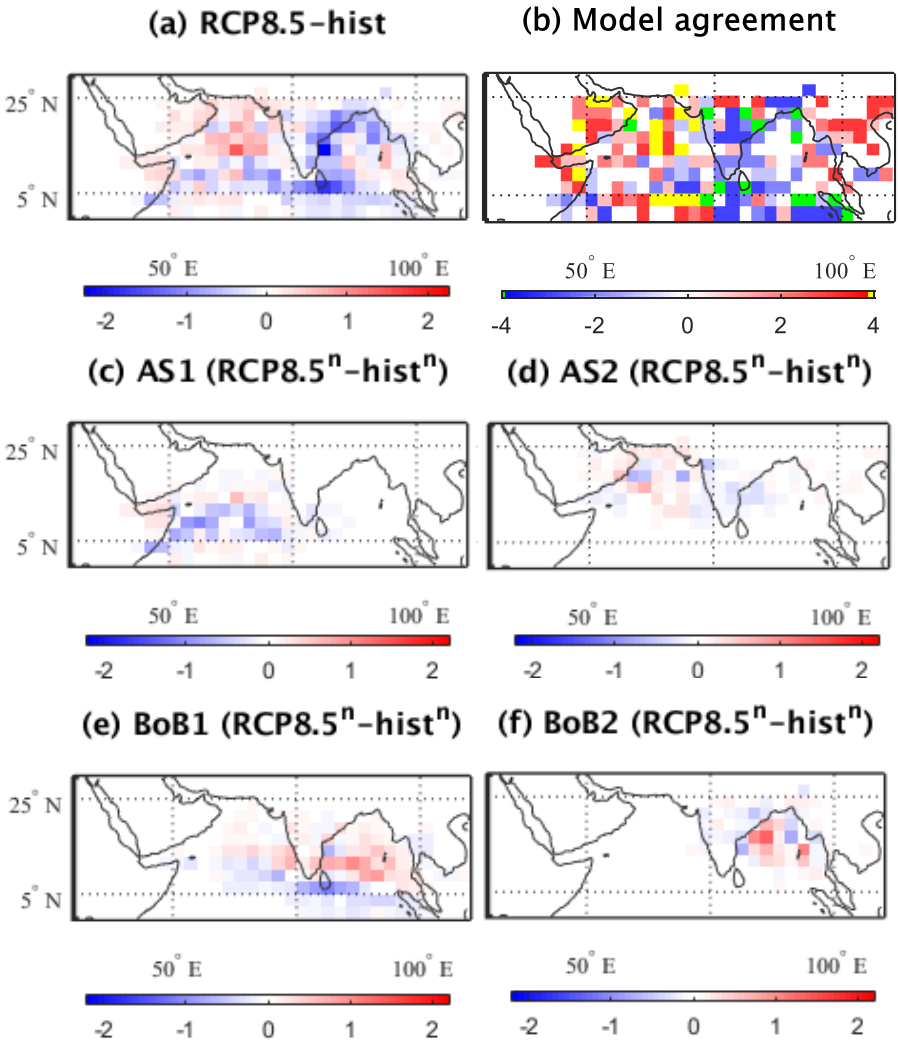

Fig. 5: (a) Projected change in TC track density (per decade) between RCP8.5 and historical CMIP5 simulations, given by a mean of four independent models (4-M). (b) Model agreement on the projected sign of change (out of a total of 4 models). (c-f) as in (a) but for individual clusters, with the number of TCs held fixed. Red grid boxes indicate a projected increase in track density under RCP8.5.